Global Journal of Science Frontier Research: a Physics and Space Science
Volume 23 Issue 10 Version 1.0 Year 2023
Type: Double Blind Peer Reviewed Interenational Research Journal
Publisher: Global Journals
Online ISSN: 2249-4626 & Print ISSN: 0975-5896

Unlocking Galactic Mysteries: Relativistic Insight into Orbital Hyper-Speeds and Dark Matter in Gas-Rich Galactic-Halos

By Tsutomu Kambe & Masanori Hashiguchi

University of Tokyo

Abstract- This study is a novel approach to the cosmological issue of the *dark matter* effect observed in gas-dominated galaxies in rotation. A possible physical mechanism is investigated to produce the hyper orbital-speeds in outer halo parts of galaxies. In the galactic space, gas clouds are abundant. Motion of the gas-clouds is viewed as a flow of a continuous fluid in curved space with gravity. Dynamical motions of the space-fluid are studied by Fluid Dynamics extended to the one of a relativistic gravitational field. The fluid flow to be studied in relativistic gravity field is reinforced by the *fluid gauge theory* equipped with a background (*dark*) gauge field. The stress-energy tensor in the general relativity is revised to take account of intrinsic nature of stress field by generalizing the isotropic pressure to an *anisotropic* stress field. Present study takes a new double-sided approach both dynamically and physically. Namely a gauge-field is newly incorporated in the system as a dynamical term, and the system is studied under a new mechanism of the *anisotropic* stress fields.

GJSFR-A Classification: *LCC Code: QB980-991*

Strictly as per the compliance and regulations of:

Unlocking Galactic Mysteries: Relativistic Insight into Orbital Hyper-Speeds and Dark Matter in Gas-Rich Galactic-Halos

Tsutomu Kambe [α] & Masanori Hashiguchi [σ]

ABSTRACT

This study is a novel approach to the cosmological issue of the *dark matter* effect observed in gas-dominated galaxies in rotation. A possible physical mechanism is investigated to produce the hyper orbital-speeds in outer halo parts of galaxies. In the galactic space, gas clouds are abundant. Motion of the gas-clouds is viewed as a flow of a continuous fluid in curved space with gravity. Dynamical motions of the space-fluid are studied by Fluid Dynamics extended to the one of a relativistic gravitational field. The fluid flow to be studied in relativistic gravity field is reinforced by the *fluid gauge theory* equipped with a background (*dark*) gauge field. The stress-energy tensor in the general relativity is revised to take account of intrinsic nature of stress field by generalizing the isotropic pressure to an *anisotropic* stress field. Present study takes a new double-sided approach both dynamically and physically. Namely a gauge-field is newly incorporated in the system as a dynamical term, and the system is studied under a new mechanism of the *anisotropic* stress fields.

Regarding the dark-matter effect, a strong evidence was found by McGaugh-Lelli-Schombert (2016), that shows a correlation between the observed radial acceleration and the gravitational acceleration predicted by observed baryon distribution within galaxies. Present study confirms the same correlation, which is predicted by the theory of fluid dynamics. The excellent matching of the theoretical prediction with the observation implies that the present approach has captured an essential aspect of the Dark Matter effect. The theory predicts both of the stellar objects and gas clouds in the galactic halos moving at hyper-speeds.

The dark matter effect is created by the action of the gauge field $\boldsymbol{a}$. The gauge field is determined by an equation in which the field $\boldsymbol{a}$ is excited by the current flux defined with the product of fluid density ρ and fluid velocity $\boldsymbol{v}$, and the degree of excitation of $\boldsymbol{a}$ is controlled by a field parameter $\mu_{\rm F}$. It is found by numerical study that a dimensionless index parameter $\kappa \propto \mu_{\rm F}/G$ plays a key role (G the gravity constant) to create sufficiently strong gauge field $\boldsymbol{a}$ which produces the hyper orbital-speeds in galactic halos. Thus the galactic inner space is connected smoothly to the outer space, based on the physics.

I. Introduction

In the outer halo parts of most galaxies exist gas clouds abundantly. Although stars are very sparse there, the halo is dominated by rarely observable gas-clouds. Actually, considerable portion of total mass of the galaxy exists there. In addition, speeds of their orbital motion are very high of the order of 200 $\sim$ 300 km$\cdot$ s^{-1}, and the gas clouds distribute over huge spatial scales. The dynamical motion of such space-fluids is likely governed by a new mechanism. Study of the motion and dynamics of such an exotic fluid should be approached in an innovative way.

Recently, McGaugh *et al.* [1] discovered a notable dynamical and mathematical facet of rotationally supported galaxies, on the basis of their observational studies on hundreds of galaxies with different morphology, masses, sizes and gas fractions, They found a universal law, implying that the rotational motions of disk galaxies are determined entirely (in a statistical sense) by the baryonic (hence visible) matters in the galaxies, even if the disks are filled with unknown dark matters. This hints *strong* connection between the observable baryonic matters and the physics producing the galactic orbital motions.

Let us take a typical galaxy supported by rotation. From the orbital velocity $V(R)$ observed at a distance R from the galactic center, its centripetal acceleration A_c (radial acceleration to the galactic center) is given by

$$A_c = V^2/R. \tag{1}$$

On the other hand, the gravitational potential Φ_g is estimated by the Poisson equation for Φ_g: $\nabla^2\Phi_g = 4\pi G\,\rho_{\rm bar}$,

Author α: Former Professor, University of Tokyo.
Author σ: Guest Scholar, Meiji University (Meiji Institute, Advanced Study of Mathematical Sciences), Tokyo. e-mail: kambe@ruby.dti.ne.jp

Global Journal of Science Frontier Research (A) Volume XXIII Issue X Version I Year 2023
1

once the baryonic mass density $\rho_{\rm bar}$ is given as a function of position from observation of the galaxy. Using the potential Φ_g found from the equation, the absolute value of gravitational acceleration A_g is given by

$$A_g = |\partial\Phi_g/\partial R|. \tag{2}$$

toward the gravity center. McGaugh *et al.* [1] succeeded in extracting a fitting curve from observations which connects average values of A_c and A_g, expressed as

$$A_c = \mathcal{F}(A_g) \equiv \frac{A_g}{1-e^{-\sqrt{A_g/A_\dagger}}}, \tag{3}$$

where $A_\dagger \approx 1.20\times10^{-10}\,\mathrm{m\,s^{-2}}$.

The functional relation (3) implies *strong* connection between the baryonic gravity acceleration A_g and the physics that generates the observed A_c. Observations show $A_c > A_g$ in general, leading to the following $A_{\rm DM}$:

$$A_c - A_g = A_{\rm DM} \quad (>0). \tag{4}$$

Non-zero $A_{\rm DM}$ is regarded as the *dark matter effect*.

In the solar system, a rough estimate for the Earth (at $R = 1au$ from Sun) or the Neptune gives, respectively, $A_g^E \approx 6\times10^{-3}\,\mathrm{m\,s^{-2}}$, or $A_g^N \approx 6\times10^{-6}\,\mathrm{m\,s^{-2}}$. Both are much larger than $A_\dagger$, implying $A_c \approx A_g$ in the solar system. However, further outward, the Oort clouds are known and thought to occupy a vast space somewhere between the distance of order 10^3 *au* from the Sun to as far out as 50×10^3 *au* (0.79 ly) or even further out. At a representative position $R_O = 0.9\times10^4 au$ within the Oort cloud, one estimates $A_g^O \approx 1.2\times10^{-11}\mathrm{m\,s^{-2}}$ which is smaller than $A_\dagger$ by 10^{-1}. The curve (3) predicts significant deviation of A_c from A_g there, and a dark matter effect is expected present in case of galactic halos.

The present paper is an effort to clarify how the term $A_{\rm DM}$ is accounted for with a physical mechanism.

II. Tully-Fischer Law, Implied By The Fitting Curve

The rotation curve $V(R)$ of galactic orbital motion keeps high values at large distances R from the gravity center and becomes nearly flat instead of falling. This was recognized as early as the 1950s [2]. Later, it was updated from observation by the law, *Tully-Fischer relation* [3]: $M_{bar} \propto (v_H)^p$ with $p = 3.5 \sim 4$, even in the case of presence of dark matter, where M_{bar} is the total baryonic mass of the galaxy and v_H the hydrogen atomic velocity at outer halo part of a galaxy. Observed values of v_H are very high, of the order of $200 \sim 300$ km$\cdot$ s^{-1}.

The law (3) says how the centripetal acceleration A_c is related to the gravitational acceleration A_g. Looking at the lower end of the A_g value, the behavior of the curve is found to be consistent with the Tully-Fischer relation. Assuming $|A_g/A_\dagger| \ll 1$, its right-hand side is given approximately by $(A_g\,A_\dagger)^{1/2}$. Using $A_c \equiv (v_H)^2/R$ and $A_g \propto M_{bar}/R^2$ as $R^{-1}\to 0$, the fitting curve (3) implies $M_{bar} \propto (v_H)^4$, consistent with the Tully-Fischer relation. Mysteriously, the gas velocity v_H at the outer halo is determined by the magnitude of whole baryonic mass M_{bar} only. It appears that internal detailed distribution of luminous masses does not influence on the global dynamics determining v_H. The Hydrogen atoms seem to be telling a mystery from the cosmic space.

III. Theory

To investigate such an exotic space fluid, the physical approach to be taken should be innovative. Observed speeds of gas clouds in the galaxy halos are very high, and the space fluids are distributed over a huge spatial scales of tens of kpc where the space is slightly curved under the gravity. The motion and dynamics of such a fluid should be studied with a renewed approach.

a) Gravity-space Fluid Dynamics and equations

Theory of fluid mechanics in *flat* space is extended to that in *curved* space with gravity. At the same time the flow filed is *strengthened* by a new theory [4], which extends the *isotropic* pressure field to general *anisotropic* stress field. This extension is carried out by incorporating the *fluid gauge theory* (*FGT* in short, summarized in Appendix A). This theory reinforces the flow fields by introducing a background *gauge field* a_ν ($\nu = 0,1,2,3$, by *4-d* spacetime notation). The field a_ν is *dark* since it is a background field. The flow field is strengthened in two aspects. The gauge field not only ensures the mass conservation of fluid flows [5], but also assists the flow field to become receptive to more complex fields. This is enabled by the transition of its stress field σ_{jk} *from* the simple *isotropic* pressure $p\delta_{jk}$ valid in quiet states of slow motion *to* more general *anisotropic* stress field M_{jk} functioning in turbulent flow states. See the note [6] for its explanation by analogy. No energy dissipation is caused by the addition of the gauge field within the combined system of flow field and gauge field (see Kambe [5], §5). This improvement enables appropriate description for turbulent high-speed motions within galactic halo space.

Weak field form of equation of motion: Following the scenario of general relativity faithfully, the recent study [7] has succeeded in deriving the equations of *Gravity-space Fluid Dynamics* by incorporating the *FGT* terms into the equation of fluid motion in curved space.

Its weak field form is represented by

$$\rho\,\hat{\nabla}_t\,\boldsymbol{v} = -\nabla\mathcal{P} + \rho\,\boldsymbol{e} + \rho\,(\boldsymbol{v}\times\boldsymbol{b})\,, \tag{5}$$

$$\hat{\nabla}_t\boldsymbol{v} \equiv \mathrm{D}_t\boldsymbol{v} + \nabla\Phi_g = \partial_t\boldsymbol{v} + (\boldsymbol{v}\cdot\nabla)\boldsymbol{v} + \nabla\Phi_g, \tag{6}$$

(from §5 of Kambe [7]), where $\hat{\nabla}_t\boldsymbol{v}$ denotes the relativistic *covariant derivative* of the fluid velocity $\boldsymbol{v}$ with respect to time t in the curved space of gravity field Φ_g,

and $\mathrm{D}_t = \partial_t + \boldsymbol{v}\cdot\nabla$ with $\nabla = (\partial_i)$, $i = 1,2,3$. See the note [8] for the significance of the terms $(\boldsymbol{v}\cdot\nabla)\boldsymbol{v}$ and $\nabla\Phi_g$ of the last expression of (6).

Using the 3-space notation $\boldsymbol{a} = (a_1, a_2, a_3)$, the 4-gauge-field a_ν is rewritten in the form $(\phi, \boldsymbol{a})$. Then we introduce new 3-vectors, $\boldsymbol{b}$ and $\boldsymbol{e}$, by

$$\boldsymbol{b} \equiv \nabla\times\boldsymbol{a}, \qquad \boldsymbol{e} \equiv -\partial_t\boldsymbol{a} - \nabla\phi_a, \tag{7}$$

where $\boldsymbol{b}$ and $\boldsymbol{e}$ constitute a pair of *fluid* Maxwell fields: fluid magnetic vector $\boldsymbol{b}$ and electric vector $\boldsymbol{e}$.

On the right-hand side of (5), the term $\nabla\mathcal{P}$ is expressed by $\rho\nabla h$ in *dissipation-free* motions [9]. Substituting the relation $\nabla\mathcal{P} = \rho\nabla h$ on the right-hand side of (5), it is seen that all the terms of (5) are multiplied by the density ρ. Hence, the factor ρ can be eliminated at all the terms in (5). Using (6), the equation (5) reduces to

$$\mathrm{D}_t\boldsymbol{v} + \nabla\hat{\Phi}_g = -\partial_t\boldsymbol{a} + \boldsymbol{v}\times\boldsymbol{b}, \tag{8}$$

where $\hat{\Phi}_g \equiv \Phi_g + h + \phi_a$, with ∇h and $\nabla\phi_a$ absorbed to the gravity term $\nabla\Phi_g$ as negligibly small contributions. The last term $\boldsymbol{v}\times\boldsymbol{b}$ of (8) is the fluid Lorentz-force deduced from the *anisotropic* stress field M_{jk} (analogous to the electromagnetic Maxwell stress).

Note that the equation (8) represents a balance among four different kinds of acceleration. The advantage of such representation will be utilized in the present investigation of the dark matter issue below. In fact, the study of McGaugh *et al.* [1] is presented with this approach, *i.e.* a balance relation among different kinds of acceleration.

b) Dynamical balance within a disk galaxy

Let us consider a particular disk-galaxy, which is rotating around the center in steady-state, so we have $\partial_t\boldsymbol{v} = 0$ in (6) and $\partial_t\boldsymbol{a} = 0$ in (8). The galaxy is keeping its *axisymmetric* form and represented with cylindrical polar coordinates (Z, R, ϕ), where the plane $Z = 0$ coincides with the disk and described with the polar coordinates (R, ϕ). The galaxy center is at $R = 0$. Here we assume that its rotating motion is represented by the following particular axisymmetric fields: $\boldsymbol{v} = (0, 0, V(R))$ and $\boldsymbol{a} = (0, 0, A(R))$.

The radial component of $\mathrm{D}_t\boldsymbol{v}$ in (8) is given by $(\mathrm{D}_t\boldsymbol{v})_R = ((\boldsymbol{v}\cdot\nabla)\boldsymbol{v})_R = -V^2/R$. For *steady axisymmetric* motion, the radial component of the equation (8) is now expressed with three terms on the plane $Z = 0$:

$$-V^2/R + \partial_R\Phi_g = (\boldsymbol{v}\times\boldsymbol{b})_R, \tag{9}$$

which represents balance among the three main terms: centripetal acceleration $-V^2/R$, gravitational acceleration $-\partial_R\Phi_g$, and the Lorentz acceleration $(\boldsymbol{v}\times\boldsymbol{b})_R$, all toward the center, where the variables are governed by:

$$\nabla^2\Phi_g = 4\pi G\,\rho, \tag{10}$$

$$(\boldsymbol{v}\times\boldsymbol{b})_R = V\,b_Z = VR^{-1}\,\partial_R(RA), \tag{11}$$

$$\nabla\times\boldsymbol{b} = \mu_{\mathrm{F}}\,\rho\,\boldsymbol{v}, \quad \boldsymbol{b} = \nabla\times\boldsymbol{a}. \tag{12}$$

Note that a field parameter μ_{F} is introduced in (12). We will see below that it plays an important role in the galaxy dynamics. It is of significance to recognize that the equation (9) expresses the same relation as the equation (4) if the signatures of all three terms are reversed. Namely, the equation (9) is just another expression of the equation $A_c - A_g = A_{\mathrm{DM}}$ of (4).

This recognition encourages to define the background gauge field term $A_{\mathrm{BF}} \equiv |(\boldsymbol{v}\times\boldsymbol{b})_R|$ as the agent which bridges the observational gap between A_c and A_g. Thus we find the following expression:

$$(\boldsymbol{v}\times\boldsymbol{b})_R\ (<0), \quad A_{\mathrm{BF}} = |(\boldsymbol{v}\times\boldsymbol{b})_R|, \tag{13}$$

predicting that the representation (13) fills the gap between the two observational values $A_c = V^2/R$ and $A_g = |\partial\Phi_g/\partial R|$.

What is implied by (13) has a profound significance. In fact it is astonishing. Firstly, the following section IV will present the evidence that the above formulation is successful and show that the curve (3) obtained from observations can be reproduced by the present theory. Namely, the theory predicts *bridging* of the observational gap between A_c and A_g. This alone is innovative enough. However, another point to be given later is much more fundamental from the physics point of view (see §V).

IV. Comparison between Observation and Theory

Now we have arrived at the stage of comparison between the observational triplet $[A_c, A_g, A_{\mathrm{DM}}]$ estimated by the curve (3) and the new theoretical triplet $[A_{\mathrm{obs}}, A_{\mathrm{grav}}, A_{\mathrm{BF}}]$ estimated according to the present formulation, where

$$A_c \equiv A_{\mathrm{obs}} = V^2/R, \tag{14}$$

$$A_{\mathrm{grav}} = |\partial_R\Phi_g|, \qquad A_{\mathrm{BF}} = |VR^{-1}\,\partial_R\Psi|, \tag{15}$$

where $\Psi \equiv RA$. See (11) for the last term A_{BF}.

The computation starts from the initial condition that the rotation curve $V = V(R)$ is given by the observations, on every galaxy investigated. Hence we have $A_c \equiv A_{\mathrm{obs}}$. See §V D for the details of computation.

Regarding the numerical estimations, four sample galaxies are chosen: NGC3198, NGC7814, NGC6503 and

NGC3741. The first NGC3198 is an example galaxy to show how the comparisons are carried out. Remaining three are chosen as representative galaxies to show different structure and morphology. Present numerical estimates will disclose amazing dynamical features of galaxies and the function of fluids in galactic space.

Theoretical base of the comparison is the equation (9) derived from the Gravity-space Fluid Dynamics (5).

a) An example galaxy NGC3198 and its MLS-plot

The NGC 3198 (Figur 1) is a barred spiral galaxy in the constellation Ursa Major approximately 47 million light years away. NGC 3198 is located in the Leo Spur, which is part of the Virgo Supercluster,

Figure 2 shows the rotation velocity of the galaxy *NGC 3198* along the radial distance R (kpc) from its center (1 kpc$= 3.1 \times 10^{19}$m). The curve marked with d is the one of observed velocity (km/s), while the curve f denotes the velocity obtained from the computed gravitational potential $\Phi_g(R)$, and the curve e denotes the velocity estimated theoretically from the fluid Lorentz acceleration $|(\boldsymbol{v}\times\boldsymbol{b})_R| = VR^{-1}\,|\partial_R(RA)|$ from (11). The last was derived from the anisotropic stress term through the background gauge field $\boldsymbol{a} = (0, 0, A(R))$. It is seen in the

Fig. 1: Galaxy NGC3198 (GALEX image, *NASA*)

diagram that the curve e tends to the observed velocity d as R approaching to 32 kpc. This is what is currently known as the *dark matter* effect. However, the present theory captures it by the term $|(\boldsymbol{v}\times\boldsymbol{b})_R|$.

Successful aspect of the present study can be seen in the diagram of Figure 3, where the data points $(A_{\rm grav}, A_{\rm obs})$ computed from NGC3198 (Fig.2) are given with the blue points of c. The points c overlap quite well with the curve a, although certain minor undulation is seen relative to the curve a. The undulation may signal that the parameter $\mu_{\rm F}$ of (12) is not a strict constant but a scalar function depending slightly on domains.

Present agreement between astronomical observation and theoretical analysis is really notable. In fact, the fitting curve $A_c = \mathcal{F}(A_g)$ of (3) was found by McGaugh, Lelli & Schombert [1] from observational data. They extracted the curve from a set of about two hundred. Hence the diagram plot of $(A_{\rm g}, A_{\rm c})$ such as Fig.3 is called the "***MLS-plot***" in the present paper. An equivalent fitting curve was confirmed by Sofue [10] (and *private communication*) from the observation data of about five hundred of galaxies .

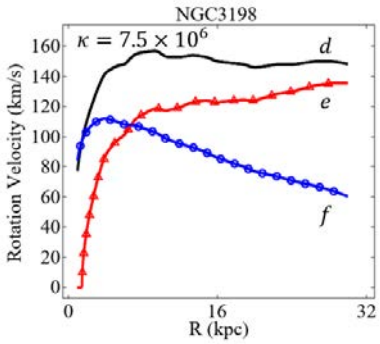

Fig. 2: NGC3198: Distributions of rotation velocities with respect to R with the unit kpc$= 3.1 \times 10^{19}$m, where d is the observed velocity V_d, while e and f are velocities V_e and V_f respectively estimated theoretically from $V_e = \sqrt{R\,A_{\rm BF}}$ (from fluid Lorentz acceleration) and $V_f = \sqrt{R\,A_{\rm grav}}$ (from gravitaional acceleration). It is seen: $V_d^2 \approx V_e^2 + V_f^2$. The velocity data were obtained with $\kappa = 7.5\times10^6$.

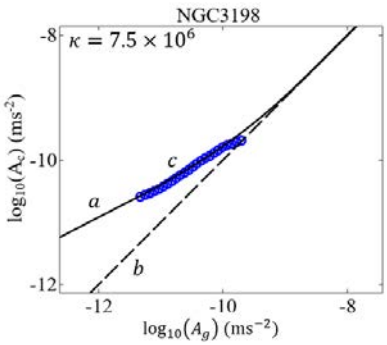

Fig. 3: *MLS-plot* (the lines a and b), overlapped with the blue data points c of Galaxy NGC3198. The ordinate is $\log_{10}(A_c)$, and the abscissa $\log_{10}(A_{\rm g})$ with the unit m/s^2 for both $A_{\rm obs} = A_c$ and $A_{\rm grav} = A_g$. Curve a: $A_c = \mathcal{F}(A_g)$ of (3); Line b: $A_c = A_g$; Blue data points c: $R = [1, 30]$ kpc with the right end at $R = 1$kpc and the left end at $R = 30$kpc.

The agreement between observation and theory tells that a new physics is working by the action of the background gauge field $\boldsymbol{a}$, which is excited by the high-speed current field $\rho\boldsymbol{v}$ of the space fluid. Typical magnitudes of the velocity $|\boldsymbol{v}|$ are observed to take values of order 10^2 km/sec at most halos of galaxies.

b) Three Representative types of Galaxies

Three sample galaxies are examined here: NGC7814, NGC6503 and NGC3741, representing different structure and morphology: *Bulge-dominated, Disk-dominated*, and *Gas-dominated* (according to [1]). Present numerical estimates will in fact show that the three galaxies are characterized with different values of the dimensionless index parameter κ defined by the equation (29).

In §V E given below, it is seen that a dimensionless parameter $\kappa \propto \mu_F/G$ plays a role of an index characterizing relative importance of the fluid current flux $\rho \boldsymbol{v}$ to the gravity effect $\partial_R \Phi_g$.

(I) NGC7814 (*Bulge-dominated spiral*) :

NGC7814 (Figure 4) is a spiral galaxy about 40 million light-years away in the constellation Pegasus. It has a bright central bulge and a bright halo of glowing gas extending outwards into space. (Also known as the *little sombrero*.) The cloud-rich spiral arms appear as dark streaks. They consist of gas clouds that absorb and block light from the galactic disk behind it. The view of this NASA/ESA HST image would be impressive even without NGC 7814 in front; nearly all the objects seen in this image are galaxies as well.

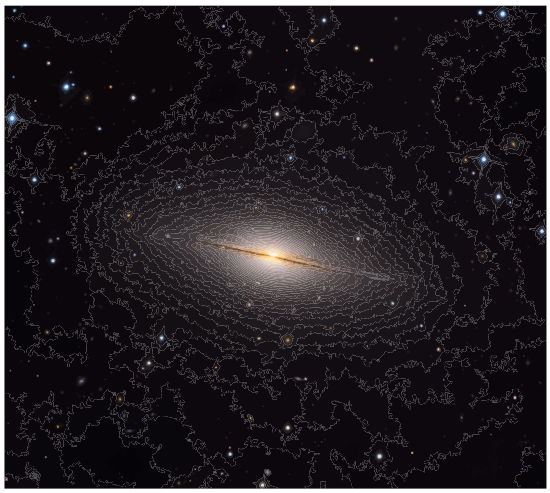

Fig. 4: Galaxy NGC7814: The galaxy is seen edge-on (*NASA/ESA Hubble Space Telescope image*).

To compare with the observed finding represented by the fitting curve (3), computational study has been carried out on this galaxy by using the system of equations (9) and (10) $\sim$ (12). The results are given by a pair of diagrams, one analogous to Fig.3 of *MLS-plot* and the other analogous to Fig.2 for velocity curves. Those are shown in the Figure 7 by the *leftmost* diagrams of both upper and lower arrays (rows) noted with NGC7814 where the parameter κ was 1.5×10^6.

Remarkably, the data points c of Galaxy NGC7814 overlap quite well with the *fitting curve* a, amazingly, the range of R examined being $[8, 20]$ (kpc).

(II) NGC6503 (*Disk-dominated spiral*):

The galaxy NGC 6503 (Figure 5) lies about 18 million light-years away at the edge of an empty patch of space called the *Local Void*. The dwarf galaxy spans 30,000 light-years and lies in the constellation of the Dragon.

To compare with the curve (3), a computational study was carried out by using the system of equations (9) $\sim$ (12). The results are given by a pair of diagrams, shown in the Figure 7 by the *central* diagrams of both upper and lower arrays (rows) noted with NGC6503 where the parameter κ was 1.9×10^7 which is larger than the previous value of NGC7814.

Agreement with the fitting curve a is excellent, the range of R examined being $[8, 22]$ (kpc).

(III) NGC3741 (*Gas-dominated faint-spiral*):

The NGC 3741 (Figure 6) is an unusual galaxy in several aspects. It has a disk of neutral hydrogen (HI) that is extremely wide, extending some 23,000 light-years (7 kpc). NGC 3741 is a galaxy in the constellation *Ursa Major*, located at a distance of about 10 million light-years (3.2 Mpc). It is relatively undisturbed by other galaxies. The disk is symmetrically warped. Since a mass-to-light ratio is $M_T/L_B \sim 149$, *it is considered to be highly rich in dark matter* (dark space clouds).

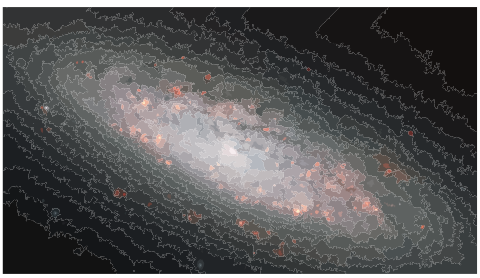

Fig. 5: Galaxy NGC6503: Its swirling spiral arms are displayed by HST Advanced Camera for Surveys, where bright (red) regions of gas are seen scattered through its spiral arms and bright (blue) regions contain stars that are forming. Dark brown dust areas are in the galaxy's arms and center. (*NASA/ESA Hubble Space Telescope image*).

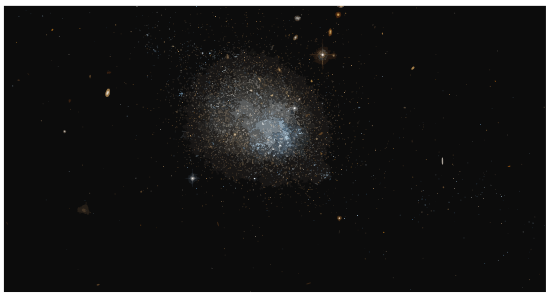

Fig. 6: Galaxy NGC3741: Speckling of stars extending to the upper left and lower right of this galaxy are seen faintly (not clearly in this print). It is tempting to call them spiral arms or attempting at spiral arms. (Hubble Space Telescope image, Wikipedia "NGC 3741")

A computational study was done and compared with the fitting curve. The results are given by a pair of diagrams, shown in Figure 7 by the *rightmost* diagrams of both upper and lower arrays (rows) noted with NGC3741 where the parameter κ was 3.7×10^8 which is larger than the previous values of NGC7814 and NGC6503.

The left part of the data points c overlap with the fitting curve a, while the right part tends to the line b (where $A_c = A_g$). The range of R examined is $[1, 6]$ (kpc). The left end corresponds to the outer part $R =$

6 (kpc), while the right part tends to the inner part. The right part implies that the inner part of the galaxy NGC3741 deviates from standard galaxies, hinting that NGC3741 may be an immature galaxy.

All the planets of the Solar system drop on the line b (*i.e.* $A_c = A_g$). Hence, no dark matter issue has been raised in the Solar system.

Following subsection **C.** summarises the above three galaxies, concerning what is implied by the difference of the index parameter value κ.

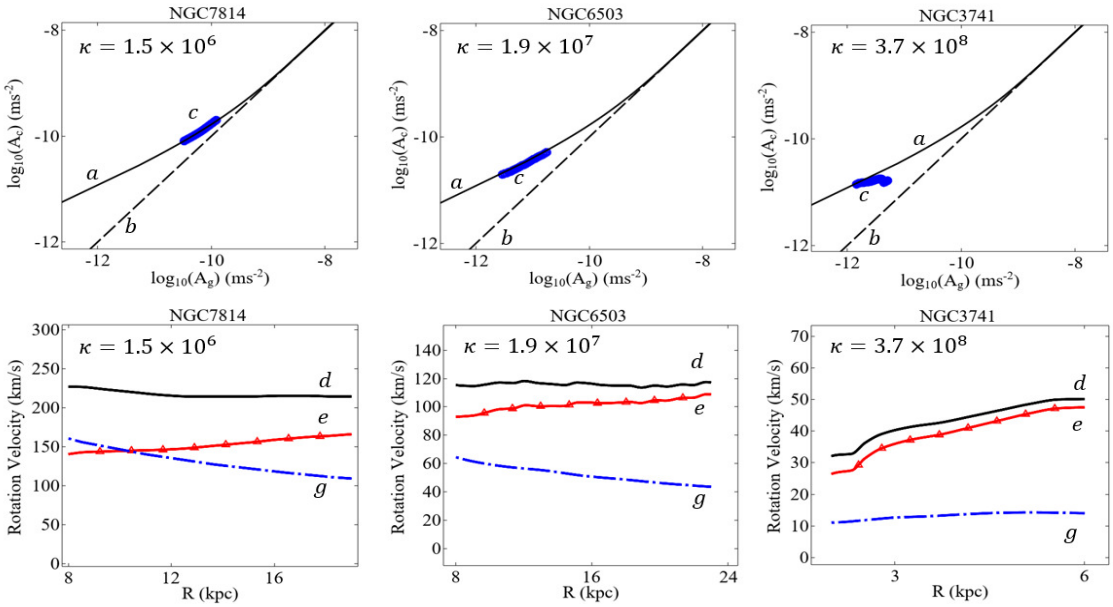

Fig. 7: *Upper Diagrams*: The MLS-plot for NGC7814, NGC 6503, and NGC3741 from the left, where the curves labeled with a and b are the same as those of Fig.3, while the curves c denote the data points corresponding to each galaxy of the diagram.

Lower Diagrams: Distributions of rotation velocities *vs.* the radial distance R, where the label d denotes the observed velocity V_d, while the label e denotes the velocity V_e estimated from $V_e = \sqrt{R\, A_{\rm DM}}$ (from the fluid Lorentz acceleration) as of Fig.2, and the label g denotes the velocity V_g given by McGaugh *et al.* [1] as the baryonic mass model. It is seen: $V_d^{\,2} \approx V_e^{\,2} + V_g^{\,2}$. The numerical data of the present work were obtained with $\kappa = 1.5 \times 10^6$ (NGC7814), 1.9×10^7 (NGC6503) and 3.7×10^8 (NGC3741).

c) What is Implied from Three Types of Morphology

The three galaxies NGC7814, NGC6503 and NGC3741 examined in the previous **B** were chosen by the difference of morphology and structure gained from astronomical observations. By the present computation analyses, it is remarkable to find that the difference is evidenced by numerical values of a dimensionless parameter κ defined in the next §V. Namely, as given in the Table I, the three galaxies are characterized in the order of magnitude of κ: $O(10^6)$ for NGC7814 (a bulge-dominated spiral); $O(10^7)$ for NGC6503 (a disk-dominated spiral), and $O(10^8)$ for NGC3741 (gas-dominated faint-spiral).

Table 1: **Dimensionless parameter $\kappa = c^2\, \mu_{\rm F}/4\pi G$ characterizing galaxies**

	NGC7814	NGC6503	NGC3741	NGC3198
κ	1.5×10^6	1.9×10^7	3.7×10^8	7.5×10^6

V. Details of Theory & Computation

a) How the Gauge Field is Excited

The mathematical advantage of the present theory is the equation (9) giving the term $A_{\rm DM}$ the expression $-(\boldsymbol{v} \times \boldsymbol{b})_R$ explicitly where the term $\boldsymbol{b} = \nabla \times \boldsymbol{a}$ depends on the FGT gauge field $\boldsymbol{a}$. By the equation (12), the field $\boldsymbol{a}$ is determined by $\nabla \times (\nabla \times \boldsymbol{a}) = \mu_{\rm F} \rho\, \boldsymbol{v}$, where the right-hand source term depends on the *fluid current density* $J_{\rm F} \equiv \rho\, \boldsymbol{v}$. In addition, the forcing is controlled by the parameter $\mu_{\rm F}$. This is an innovative point.

b) Significance of the Theory

Present *fluid gauge theory* for a perfect fluid represents a broader class of flow fields than the current Eulerian field by incorporating the background field $\boldsymbol{a}$, and covers a broader family of flow fields of a perfect fluid.

In the presence of the gauge field $\boldsymbol{a}$, the governing equation was given by (8), which is rewritten here again,

$$\mathrm{D}_t \boldsymbol{v} + \nabla \hat{\Phi}_g = -\,\partial_t \boldsymbol{a} + \boldsymbol{v} \times \boldsymbol{b}, \ (\equiv \hat{\boldsymbol{f}}_a). \qquad (16)$$

Note that this includes the Lorentz-type acceleration $\boldsymbol{v} \times$

$\boldsymbol{b}$ in fluid flows which is neutral electrically. The role of charge density is played by the mass density ρ here.

c) Fluid Lorentz Acceleration $\boldsymbol{v} \times \boldsymbol{b}$

The equation (16) shows that the fluid Lorentz acceleration $\boldsymbol{v} \times \boldsymbol{b}$ depends on the velocity $\boldsymbol{v}$, acting perpendicularly to the 3-vector $\boldsymbol{v}$. This is contrasted with the gravity acceleration which is directed to the gradient of a scalar potential function Φ_g (but the direction reversed). In this sense, the action of $\boldsymbol{v} \times \boldsymbol{b}$ is twisted to the perpendicular direction, unlike the parallel action of $\nabla\Phi_g$.

It is helpful to remember the case of Kundt-tube experiment [7, 11] to get an insight into the action of the gauge field $\boldsymbol{a}$. "*The gauge field within the Kundt-tube is not visible, yet creates visible dust-striations mechanically*". This insight applies analogously not only to the present gauge field $\boldsymbol{a}$, but also to the gravitational potential Φ_g as well. The gauge field $\boldsymbol{a}$ (the gravitational potential Φ_g) is not visible, yet the action of $\boldsymbol{v} \times \boldsymbol{b}$ (of $\nabla\Phi_g$) creates a visible dynamical effect.

In addition, the acceleration $\hat{\boldsymbol{f}}_a$ on the right-hand side depends on the time derivative $\partial_t \boldsymbol{a}$ and rotational term $\boldsymbol{b} = \nabla \times \boldsymbol{a}$. Hence the $\hat{\boldsymbol{f}}_a$ would become significant in turbulent flow fields that are time-dependent and rotational. The fluid acceleration $-\nabla(h + \phi_a) + \hat{\boldsymbol{f}}_a$ (in addition to the gravity acceleration $-\nabla\Phi_g$) is regarded as a generalization of the pressure force $-\nabla p$,

d) Computation Scheme of the Present Study

When we try to study the physics and dynamics of galaxy rotations, reliable astronomical laws or equations are not so many. Fortunately, we have two laws, which can be used in the present study of galaxy rotation and dark matter issue. In addition nowadays, rotation curves $V = V(R)$ are available for hundreds of galaxies (*e.g.* McGaugh *et al.* [1], Sofue [10]). In our study under the assumption of steady rotation of axisymmetric galaxies, the velocity $\boldsymbol{v}$ and gauge field $\boldsymbol{a}$ are represented by $\boldsymbol{v} = (0, 0, V(R))$ and $\boldsymbol{a} = (0, 0, A(R))$ respectively in the cylindrical polar coordinates (Z, R, ϕ).

The *computation scheme* is summarized here with the following ten items: (**a**) $\sim$ (**j**).

(**a**) The **first one** is the *MLS-plot* and the associated fitting curve (3) cited here again as

$$A_c = \mathcal{F}(A_g) \equiv \frac{A_g}{1 - e^{-\sqrt{A_g/A_\dagger}}}, \tag{17}$$

which was extracted as a mean curve from extensive observational data acquired by McGaugh *et al.* [1].

(**b**) **Second one** is the equation (9) representing the dynamical balance of a rotating disk of a galaxy in axisymmetric steady state (Kambe [7]), which is the balance of radial accelerations to the center on the disk $Z = 0$:

$$-V^2/R + \partial_R \Phi_g = (V/R)\ \partial_R \Psi, \tag{18}$$

where (11) is used on the right-hand side with $\Psi \equiv RA$.

(**c**) **Third one** is the given rotation curve of each galaxy:

$$V = V(R), \tag{19}$$

([1], [10], [12]). The observed curve $V(R)$ gives the initial condition to start the computation. Hence, the first term $V(R)^2/R$ of (18) is known for subsequent computations.

(**d**) **Fourth**: The equation (18) includes two field variables Φ_g and $\Psi = RA$, governed by (10) and (12):

$$\nabla^2 \Phi_g = R^{-1} \partial_R (R\, \partial_R \Phi_g) + \partial_Z^2 \Phi_g \ = \ 4\pi G\, \rho, \tag{20}$$

$$\partial_R (R^{-1} \partial_R \Psi) + R^{-1}\, \partial_Z^2 \Psi \ = \ -\mu_{\rm F}\, \rho\, V, \tag{21}$$

where the left-hand side of (21) is equal to $-(\nabla \times \boldsymbol{b})_\phi$. Regarding $(\nabla \times \boldsymbol{b})_\phi$, see the note [13].

(**e**) **Fifth**: Density distribution $\rho(Z, R)$ is assumed to decay rapidly to the Z-direction normal to the disk plane $Z = 0$. For simplicity, the density is defined with an exponential Z-factor as

$$\rho(R, Z) = h_4(Z)\, \rho_*(R), \quad h_n(Z) \equiv \exp\left[-(Z/\Delta)^n\right], \tag{22}$$

where Δ is a scale-constant, and $n = 4$ was chosen since this worked better than $n = 2$ [14].

(**f**) **Sixth**: Other field variables are represented by using the normal distribution (22) as

$$\Phi_g(Z, R) = h_4(Z)\, \Phi_*(R), \quad \Psi_g(Z, R = h_4(Z)\, \Psi_*(R),$$
$$\phi\text{-current flux: } J(Z, R) \equiv \rho\, V = h_4(Z)\, \rho_*(R)\, V(R), \tag{23}$$

on account of the linearity of the differential operators on the left-hand side of (20) and (21).

Owing to the normal function $h_4(Z)$, the terms $\partial_Z^2 \Phi_g$ and $\partial_Z^2 \Psi$ vanish on the disk plane $Z = 0$ (Appendix B). Hence the system of equations of (20) and (21) reduces to the one-dimensional problem with respect to R, since the factor $h_4(Z)$ can be eliminated from the system.

Selecting a galaxy for the target of analysis, the above system of equations (17) $\sim$ (23) are solved numerically.

(**g**) **Boundary conditions**: First, the radial section of R is chosen: $[R_1, R_2]$ with $R_1 < R_2$.

Since the present study is interested in investigating the halo, the R_2-value is chosen within the halo. Then we have $V_2 = V(R_2)$ from (19) and $A_c(R_2) = {V_2}^2/R_2$. The last yields $A_g(R_2) = \mathcal{F}^{-1}[A_c(R_2)]$ from (17). Then

$$Y \equiv \partial_R \Psi\Big|_{R_2} = \Big(-A_c(R_2) + A_g(R_2) \Big)\ (R_2/V_2)\Big|_{R_2}. \quad (24)$$

from (18). Arbitrariness of Ψ is fixed by $\Psi(R_1) = 0$.

(**h**) **Preparation of dimensionless equation for computation**: The equations (20) and (21) are solved on the disk plane $Z = 0$, under the conditions (18) and (19) and also with $\partial_Z^2 \Phi_g = 0$ and $\partial_Z^2 \Psi = 0$.

By the help of the equation (18), the system of equations (20) and (21) are reduced to a single equation. To derive it, consider (20) and (18):

$$4\pi G\, \rho_* \ = \ R^{-1} \partial_R (R\ \partial_R \Phi_g), \quad (25)$$

$$\partial_R \Phi_g \ = \ (V/R)\ \partial_R \Psi + V^2/R. \quad (26)$$

Eliminating the term $\partial_R \Phi_g$ between (25) and (26),

$$4\pi G\, \rho_* = R^{-1} \partial_R (V\, \partial_R \Psi + V^2). \quad (27)$$

The left-hand side of (27) represents the source of gravity $S_G = 4\pi G \rho_*(R)$, while the right-hand side of (21) represents the strength $S_L = \mu_{\rm F} \rho_* RV$ exciting the potential Ψ (equivalently the fluid Lorentz force). Eliminating ρ_* between (27) and (21):

$$R\, \partial_R (R^{-1} \partial_R \Psi) = -\frac{\kappa}{c^2}\ V(R)\ \partial_R (V\, \partial_R \Psi + V^2). \quad (28)$$

$$\kappa = \frac{\mu_{\rm F}}{4\pi G}\ c^2 : \ \textit{dimension-less}. \quad (29)$$

Introducing dimension-less variables $V_* \equiv V/c$, $R_* \equiv R/L$, and $\Psi_* \equiv \Psi/(cL)$ with L a scale of the galaxy. the equation (28) is converted to a dimensionless form:

$$R_*\, \partial_{R_*} (R_*^{-1} \partial_{R_*} \Psi_*) = -\kappa\, V_*\, \partial_{R_*} (\, V_*\, \partial_{R_*} \Psi_* + V_*^2). \quad (30)$$

This is a second order (ordinary) differential equation with the dimension-less parameter κ.

This equation describes the mechanism of how the gauge potential Ψ_* is excited by the rotation velocity $V_*(R)$ of the galaxy. The degree of excitation is controlled by the *dimension-less* parameter $\kappa = c^2\, (\mu_{\rm F}/4\pi G)$, proportional to the ratio $\mu_{\rm F}/G$, signifying relative strength of two excitations with $\mu_{\rm F}$ denoting excitation by current flux ρV (see (21)) and G the symbol of gravity excitation.

(**i**) **Finite element algorithm**: The equation(30) is solved by the *finite-element* method, choosing an appropriate value for the parameter κ, with the given function $V(R)$ of (19) and under the boundary conditions:

$$\Psi_* = 0 \text{ at } R_* = \frac{R_1}{L}; \ \ \partial_{R_*} \Psi_* = Y_* \text{ at } R_* = \frac{R_2}{L}, \quad (31)$$

For the derivative $\partial_R \Psi$, see (24).

From the equation (15), we find $A_{\rm BF} = |VR^{-1}\, \partial_R \Psi|$, and from (9), $A_{\rm grav} = |\partial_R \Phi_g| = V^2/R - A_{\rm BF}$. The diagram of *MLS-plot* will give $A_{\rm DM}$ when the abscissa is chosen at A_g. Setting A_g with the computed value $A_{\rm grav}$, one must compare the diagram value $A_{\rm DM}$ with the computed value $A_{\rm BF}$.

(**j**) **Iterative solving, and final outcomes**: If those two do not match, the index-parameter κ must be corrected to a new better value, and another try of computation must be done to find a better matching value. Iterative computation must be repeated until satisfactory matching is obtained between the computed curve ($A_{\rm obs}$ vs. $A_{\rm grav}$) and the curve (A_c vs. A_g) of (3).

Thus, the triplet $[A_{\rm obs}, A_{\rm grav}, A_{\rm BF}]$ of theoretical computation has been found for the four galaxies examined. Those are plotted in the diagram *MLS-plot* of Figures 3 and 7 by the data points marked with c. Matching with the curve (3) marked with a is *remarkable*.

The case of NGC3741 of Fig.7 must be given an additional remark. The data points c in the diagram at the upper right of Fig.7 tend to deflect from the curve a toward the line b of $A_c = A_g$ at its right end. The right direction of the abscissa corresponds to larger values of A_g, which means the inner direction within the galaxy. In the inner part, the gravity effect tends to dominate the gauge field effect. Recall that in the solar-planetary system, the relationship $A_c = A_g$ is almost satisfied.

e) Parameter κ as a Characterizing Index

It is found from the present numerical analyses that each galaxy is characterized by different values of the *dimensionless* index parameter $\kappa = c^2\, \mu_{\rm F}/4\pi G$ (Table I). In §IV B, we have seen three different types of galaxies:

a: 7814 (Bulge-dominated): $\kappa = O(10^6)$, $V_{\rm h} \approx 230 \frac{\rm km}{\rm s}$;

b: 6503 (Disk-dominated): $O(10^7)$, $V_{\rm h} \approx 120 \frac{\rm km}{\rm s}$;

c: 3741 (Gas-dominated): $O(10^8)$, $V_{\rm h} \approx 50 \frac{\rm km}{\rm s}$.

It is remarkable to find that the parameter κ increases by ten times from the top *Bulge-dominated spiral* galaxy, to the middle *Disk-dominated spiral* and another ten to the bottom *Gas-dominated faint-spiral*. This fact may imply that the index κ denotes the degree of the amount of gas-content or the degree of relative contribution of the rotational current of the gas component to the gravity effect within the galaxy.

Another aspect is the following. The right-hand side of (30) implies for the halos (where cV_* is approximately a constant $V_{\rm h}$) that the product $\kappa\, V_{\rm h}^2$ is approximated with a constant. This means $V_{\rm h} \propto 1/\sqrt{\kappa}$, decreasing as κ increases, as seen in the above list of (**a, b, c**).

It is noted that the dimensionless parameter κ is proportional to the ratio $\mu_{\rm F} c/(4\pi G)$. This ratio signifies relative importance of the fluid current effect $(\mu_{\rm F} \boldsymbol{v})\, \rho$ of (21) to the gravity effect $(4\pi G)\, \rho$ of (20).

VI. Conclusion

This study is a novel approach to the cosmological issue of the *dark matter* effect observed in rotating galaxies, investigating a possible physical mechanism producing hyper orbital speeds in outer halo parts of galaxies. In cosmic space, it is crucial to recognize firstly that gas clouds are abundant and free to move in galactic and inter-galactic spaces. Structure and morphology of galaxies are diverse in regard to the relative amount of dark gas-clouds to that of shining stellar objects. Usually, galaxy forms are classified as *Disk-dominated spiral*, *Gas-dominated faint spiral*, or *Bulge-dominated spiral*.

Motion of the space-clouds is viewed as a flow of continuous fluid in curved space with gravity. Dynamical motions of the space-fluid of rotating galaxies are investigated by extending *Fluid Dynamics* to that in the frame of *general relativity*. The fluid flow, which is extended to the space of relativistic field, is reinforced by the *fluid gauge theory* equipped with a background (*dark*) gauge field conditioning the current continuity. The *Gravity-space Fluid Dynamics* thus developed captures the main feature of the dark-matter effect as the action of the gauge field on the motion of space fluids. In the present formulation, the stress-energy tensor in the general relativity is revised to take account of the general nature of the stress field by extending the isotropic pressure to an anisotropic stress field.

Regarding the dark-matter effect, McGaugh-Lelli-Schombert (2016) [1] found a strong evidence, that shows existence of a functional correlation between the *observed centripetal* radial-acceleration and the *gravitational* acceleration predicted by observed baryon distribution within galaxy. This implies that the dark matter contribution is specified by the baryon distribution. But their inter-connection is mysteriously twisted between the visible matters and the physics producing the rotational motion. Present theory describes this aspect successfully and gives an explicit mathematical expression to the acceleration attributed to the dark-matter effect.

The present study takes a new double-sided approach both dynamically and physically: namely incorporating a new dynamical field of dark gauge-field $\boldsymbol{a}$ and attacking the system with a new physics using anisotropic stress fields. The *dark matter effect* is created by the action of the gauge field $\boldsymbol{a}$. The gauge field is determined by an equation in which the field $\boldsymbol{a}$ is excited by the current flux $\rho\boldsymbol{v}$. The enhanced acceleration attributed to the dark-matter effect is given by that of *fluid Lorentz* force $(\boldsymbol{v}\times\boldsymbol{b})_R$ toward the gravity center. Namely, the rotating current flux $\rho\boldsymbol{v}$ in the azimuthal direction creates the centripetal acceleration toward the center. The mechanism is twisting.

It is a central point in the present study that the mechanical balance equation (9), $-V^2/R+\partial_R\Phi_g=(\boldsymbol{v}\times\boldsymbol{b})_R$ of the galaxy dynamics, is just another expression of the equation (4) with the sign reversed: $-A_c+A_g=-A_{\rm DM}$ of the *MLS-plot*. In addition, the computations according to (10) $\sim$ (12) give the results perfectly matching the fitting curve (3) of observations. Note that the present theoretical study is based on the Gravity-space Fluid Dynamics, developed by Kambe [7].

The *MLS-plot* found by McGaugh *et al.* [1] is interpreted in the section IV A with adding the data gained by the present study, which is shown by Fig. 3. The successful matching of the present theory (9) with the observation relation (4) implies that the present approach has captured an essential aspect of the Dark Matter effect, represented diagramatically by the *MLS-plot* and expressed mathematically by the fitting curve (3). Note that both of the plot and curve were extracted from the data of hundreds of rotationally supported galaxies.

Agreement between the astronomical data and the physics data deduced from the present theory is excellent. This agreement implies that the space clouds exist abundantly in the galactic halo space and their amount is sufficient for the effective action of the fluid gauge field.

It is found from the present numerical analyses that each galaxy supported rotationally is characterized with different values of a dimensionless index parameter, $\kappa=c^2\mu_{\rm F}/(4\pi G)$. From the right-hand side of (30), it is seen that the orbital velocity $V_{\rm h}(\approx cV_*)$ in the halo increases inversely to the magnitude of κ. In addition, since $\kappa\propto\mu_{\rm F}/G$, this ratio signifies relative importance of the fluid current effect $(\mu_{\rm F}\boldsymbol{v})\,\rho$ to the gravity effect $(4\pi G)\,\rho$, as noted in §V E.

The galactic inner space is connected continuously to the deep-outer space by the mechanical help of the fluid gauge field, without presence of dark matters.

Acknowledgments

The authors would like to express thanks to Prof. Emeritus Yoshiaki Sofue (University of Tokyo) for discussions on galaxies and rotation curves.

Formatting of the present text is helped by the *Overleaf* for its creation.

Appendix A: Fluid Gauge Theory (FGT) in Flat Space, Summarized

According to the relativistic FGT theory ([4], or §2 & §5 of [7]) in flat Lorentzian space, the fluid system is described by the total Lagrangian $\mathcal{L}^{\rm FGT}$ consisting of three components, $\mathcal{L}^{\rm FGT}=\mathcal{L}_{\rm FM}+\mathcal{L}_{\rm int}+\mathcal{L}_{\rm GF}$:

$$\mathcal{L}_{\rm FM}=-c^{-1}(c^2+\bar{\epsilon}(\overline{\rho}))\,\overline{\rho}, \tag{A1}$$

$$\mathcal{L}_{\rm int}=c^{-1}j^\nu\,a_\nu\,, \tag{A2}$$

$$\mathcal{L}_{\rm GF}=-(4\mu c)^{-1}f^{\nu\lambda}\,f_{\nu\lambda}, \tag{A3}$$

$$f_{\nu\lambda}=\partial_\nu a_\lambda-\partial_\lambda a_\nu,\quad \overline{\rho}\equiv\rho\sqrt{1-\beta^2}, \tag{A4}$$

where the *overlined* values denote proper values and the Lagrangian $\mathcal{L}_{\rm GF}$ includes a free parameter μ to be fixed later (Section V):

The frst Lagrangian $\mathcal{L}_{\rm FM}$ describes a perfect fuid in motion with 4-current mass flux $j^\nu = \rho\, v^\nu$ with $v^\nu = (c, v^1, v^2, v^3)$, and the third $\mathcal{L}_{\rm GF}$ describes an action of a background gauge field a_ν so as to ensure the fluid motion to satisfy mass conservation (to be shown later), while the middle $\mathcal{L}_{\rm int}$ describes their mutual interaction between j^ν and the gauge-field a_ν.

Equations governing the system:

Variational principle is applied to $\mathcal{L}^{\rm FGT}$ to derive governing equations. The equation of motion is deduced as

$$\rho\, {\rm D}_t\, v_k = -\partial_k p + \rho\, f_{k\nu}\, v^\nu, \quad (k = 1, 2, 3). \tag{A5}$$

in the non-relativistic limit as $\beta = |\boldsymbol{v}|/c \to 0$. This is the Euler's equation with the additional term $\rho\, f_{k\nu}\, v^\nu$ on the right hand side. The first term $-\partial_k p$ came from the *isotropic* pressure stress $\sigma^{\rm I}_{jk} = -p\, \delta_{jk}$. The second is a new term that came from the *anisotropic* stress $\sigma^{\rm A}_{jk}$ to be given below.

The equation governing the gauge field a_ν is derived from the variational principle as

$$\frac{\partial}{\partial x^\lambda} f^{\nu\lambda} = \mu_{\rm F}\, j^\nu, \qquad j^\nu = (\rho c, \rho \boldsymbol{v}), \tag{A6}$$

[4], where μ of (A3) is a control parameter, hence redefined here as $\mu_{\rm F}$, which controls the degree of mutual interaction between the current j^ν and the field strength tensor $f^{\nu\lambda}$ of the background gauge field.

Thus it is seen that the fluid gauge theory represents a broader class of flow fields than the current Eulerian field. By the help of the background field a^ν, the system covers a wider family of flow fields of a perfect fluid (an inviscid fluid). In the presence of the gauge field a^ν, the governing equation is given by (A5)

The equation (A5) can be transformed to very illuminating form, represented with an equivalent 3-vector form as follows:

$$\rho\, {\rm D}_t \boldsymbol{v} = -\nabla\, p + \rho\, \boldsymbol{f}_a, \tag{A7}$$

$$\boldsymbol{f}_a = \boldsymbol{v} \times \boldsymbol{b} + \boldsymbol{e} = \boldsymbol{v} \times \boldsymbol{b} - \nabla\phi - \partial_t \boldsymbol{a}. \tag{A8}$$

Note that this includes the Lorentz-type force $\boldsymbol{f}_a$ in fluid-flow field which is neutral electrically. The role of charge density in the electromagnetism is played here by the mass density ρ.

Significance of fluid Lorentz acceleration $\boldsymbol{f}_a$

Significance of $\boldsymbol{f}_a$ is interpreted from two aspects. Firstly, as seen in (A8), the acceleration $\boldsymbol{f}_a$ is apparently independent of the mass density ρ although the $\boldsymbol{b}$-field is controlled by $\boldsymbol{j} = \rho\boldsymbol{v}$ from (A12). The $\boldsymbol{f}_a$ instead depends on the velocity $\boldsymbol{v}$ unlike the gravity acceleration, as seen from (9) and (10). In addition, it depends on the time derivative $\partial_t \boldsymbol{a}$ and rotational term $\nabla \times \boldsymbol{a}$. Hence the $\boldsymbol{f}_a$ would become significant in turbulent flow fields in which flow fields are time-dependent and rotational. The fluid Lorentz acceleration $\boldsymbol{f}_a$ is regarded as a generalization of the pressure force $-\nabla p$, as seen next.

Secondly, physical meaning of $\boldsymbol{f}_a$ may be given as follows. The force field $\boldsymbol{F}_a \equiv \rho \boldsymbol{f}_a$ is represented by the stress field $M^{\nu k}$. In fact, regarding the spatial components, the k-th component of the force $\boldsymbol{F}_a \equiv \rho \boldsymbol{f}_a$ can be written as follows $(i, k = 1, 2, 3)$:

$$(\boldsymbol{F}_a)^k = (\rho \boldsymbol{e} + \rho \boldsymbol{v} \times \boldsymbol{b})^k = -\partial_\nu M^{\nu k}, \tag{A9}$$

$$M^{0k} = c\epsilon\, (\boldsymbol{e} \times \boldsymbol{b})_k,\ M^{00} = \tfrac{1}{2}\, \epsilon\, |\boldsymbol{e}|^2 + \tfrac{1}{2}\, \mu_{\rm F}^{-1}\, |\boldsymbol{b}|^2 \equiv w_e,$$

$$M^{ik} = -\epsilon\, e_i e_k - \mu_{\rm F}^{-1}\, b_i b_k + w_e \delta_{ik}, \tag{A10}$$

where $\partial_\nu = (c^{-1}\partial_t, \partial_k)$, and $\mu_{\rm F}$ and $\epsilon = 1/(\mu_{\rm F}\, c^2)$ are parameters of flow fields, The equality $(\rho \boldsymbol{e} + \rho \boldsymbol{v} \times \boldsymbol{b})_k = -\partial_\nu M^{\nu k}$ can be shown by using (A12) and (A13). The stress tensor M^{ik} of (A10) as well as the parameters ϵ and $\mu_{\rm F}$ are analogous to the Maxwell stress tensor of electromagnetism. The term $(-\nabla\, p)^k$ on the right-hand side of (A7) can be written as $-\partial_j (p\, \delta^{jk})$, a force from the isotropic pressure stress $-p\, \delta^{jk}$. According to the *present* fluid gauge theory, the state of *isotropic* pressure stress $p\, \delta^{jk}$ of Eulerian system is extended to the state of combined *anisotropic* stress $p\, \delta^{jk} + M^{jk}$.

Equations of $\boldsymbol{a}$, $\boldsymbol{b}$ *and* $\boldsymbol{e}$: Using the 3-vector notation $\boldsymbol{a} = (a_1, a_2, a_3)$, the 4-field a_ν is rewritten as $(\phi, \boldsymbol{a})$. Then, two 3-vectors $\boldsymbol{b}$ and $\boldsymbol{e}$ are defined by

$$\boldsymbol{b} \equiv \nabla \times \boldsymbol{a}, \qquad \boldsymbol{e} \equiv -\partial_t \boldsymbol{a} - \nabla\phi, \tag{A11}$$

where $\boldsymbol{b}$ and $\boldsymbol{e}$ are introduced as a pair of *fluid* Maxwell fields in the fluid system. If the gauge field a_ν is represented as $a_\nu = \partial_\nu \Psi$, all the components $f_{\nu\lambda}$ and $f^{\nu\lambda}$ vanish. Correspondingly, both of $\boldsymbol{b}$ and $\boldsymbol{e}$ vanish.

Using the definitions (A11), the equation (A6) is transformed to a pair of equations analogous to the Maxwell equations of *Electromagnetism*. In fact, with using the relations $\boldsymbol{d} = \epsilon \boldsymbol{e}$ and $\boldsymbol{h} = \boldsymbol{b}/\mu_{\rm F}$ where $\epsilon \equiv 1/(\mu_{\rm F}\, c^2)$, the equation (A6) gives a pair of Maxwell equations:

$$-\partial_t(\epsilon \boldsymbol{e}) + \mu_{\rm F}^{-1} \nabla \times \boldsymbol{b} = \boldsymbol{j}, \qquad \nabla \cdot (\epsilon \boldsymbol{e}) = \rho. \tag{A12}$$

Definition (A11) leads to another pair:

$$\partial_t \boldsymbol{b} + \nabla \times \boldsymbol{e} = 0, \qquad \nabla \cdot \boldsymbol{b} = 0. \tag{A13}$$

Equation of current conservation: The equation of current conservation can be derived from Eq.(A6), which is directly connected to the gauge-invariant property of the Lagrangian $\mathcal{L}_{\rm GF}$. Applying the divergence operator ∂_ν on (A6), one obtains $0 = \partial_\nu \partial_\lambda f^{\nu\lambda} = \mu_{\rm F}\, \partial_\nu j^\nu$. Hence, vanishing of the last expression leads to the current conservation equation:

$$\partial_\nu j^\nu = 0, \quad \Rightarrow \quad \partial_t \rho + \nabla \cdot (\rho \boldsymbol{v}) = 0. \tag{A14}$$

Thus the third $\mathcal{L}_{\rm GF}$ ensures the *mass conservation*.

Appendix B: 3D density, distributing normal to disk

The gravity potential Φ_g is influenced naturally by 3D density distribution $\rho(Z,R)$ normal to the disk plane $Z=0$ according to the equation (10): $\nabla^2\Phi_g = 4\pi G\,\rho(Z,R)$. Let us consider the simplest case of $\rho(Z,R)$ factorized as

$$\rho(Z,R) = f(Z)\ \rho_D(R), \quad f(Z) \equiv \exp\Big[-Z^4/\Delta^4\Big], \quad \text{(B1)}$$

where the thickness Δ is assumed to be a constant for simplicity. The reason why Z^4 is used in $f(Z)$ becomes clear below. In view of the linear nature of $\nabla^2\Phi_g = 4\pi G\, f(Z)\rho_D(R)$ with respect to Φ_g, the potential $\Phi_g(Z,R)$ is also factorized as of the form $\Phi_g = f(Z)\,Q_g(R)$. Substituting this into the equation

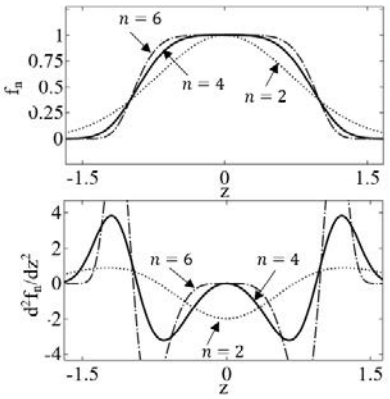

FIG. 8. The z-factor $f_n(z)$ for normal distribution: $n = 2, 4, 6$.

$\nabla^2\Phi_g = 4\pi G\, f(Z)\rho_D(R)$ and dividing both sides with $f(Z)Q_g(R)$, we obtain

$$\frac{1}{Q_g}\,\frac{1}{R}\partial_R(R\ \partial_R Q_g) + \frac{1}{f}\partial_Z^2 f = 4\pi G\ \frac{\rho_D(R)}{Q_g(R)}, \quad \text{(B2)}$$

$$f^{-1}\partial_z^2 f = (-12z^2 + 16z^6), \quad z \equiv Z/\Delta\,. \quad \text{(B3)}$$

Eliminating $f^{-1}\partial_z^2 f$ from the above two, we obtain

$$\nabla_R^2\, Q_g + (-12z^2 + 16z^6)\, Q_g = 4\pi G\,\rho_D(R), \quad \text{(B4)}$$

where $\nabla_R^2 \equiv R^{-1}\,\partial_R(R\,\partial_R\,)$. Over the galactic disk plane $z=0$, this reduces to

$$(\partial_R^2 + R^{-1}\partial_R)\ Q_g(R) = 4\pi G\,\rho_D(R). \quad \text{(B5)}$$

On the other hand, the Poisson equation (10) for the gravitational potential Φ_g can be written on the disk plane ($Z=0$) under axisymmetry as

$$(\partial_R^2 + R^{-1}\partial_R)\Phi_g + \partial_Z^2\Phi_g = 4\pi G\,\rho(Z,R)\Big|_{Z=0}, \quad \text{(B6)}$$

If the term $\partial_Z^2\Phi_g$ vanishes, we have

$$(\partial_R^2 + R^{-1}\partial_R)\Phi_g = 4\pi G\,\rho(Z,R)\Big|_{Z=0}. \quad \text{(B7)}$$

This is equivalent to the equation (B5).

Thus, it is found that the 2D axi-symmetric Poisson equation (B7) can describe the 3D density distribution as far as the normal distribution of ρ is represented at least as (B1).

Next, consider other cases such as Gaussian or $\exp[-z^n]$ distribution to the Z direction. Suppose the density is like (B1), but the $f(Z)$ factor is given by

$$f_n(z) = \exp[-z^n], \quad z = Z/\Delta. \quad \text{(B8)}$$

Then, we have

$$f_n^{-1}\ \partial_z^2 f_n = \big(-n(n-1) + n^2 z^n\big)\, z^{n-}. \quad \text{(B9)}$$

In the Gaussian case $\rho \propto e^{-z^2}\,\rho_D(R)$, we have $f_2^{-1}\ \partial_z^2 f_2 = -2 + 4z^2$, which does not vanish over the disk $z=0$. Hence, the 3D Poisson equation (B2) does not reduce to 2D problem (B7) for $n=2$. However, for even integer $n \geq 4$, the 3D equation (B2) reduces to the 2D problem (B7).

The last result is very interesting, which can be seen visually in the Figure 8.

References Références Referencias

[1] S. S. McGaugh, F. Lelli, and M. Schombert (MLS), Phys. Rev. Lett. **117**, 201101 (2016).

[2] Y. Sofue and V. Rubin (SR), ARAA **39**, 137 (2001).

[3] R. B. Tully and J. R. Fisher (TF), A A **54**, 661 (1977).

[4] T. Kambe, Fluid gauge theory, GJSFR **21**, 113 (2021).

[5] T. Kambe, New perspectives on mass conservation law & waves in fluid mechanics, Fluid Dyn. Res. **52**, 1 (2020).

[6] By analogy, this is like the *ferrocement*, a plaster reinforced with metal mesh, although it is a solid, not a fuid,

[7] T. Kambe, Relativistic exploration of dark matter effects in rotating galaxy, studied fluid-dynamically, GJSFR-A, **23 (8),** 13-27, (2023).

[8] The second and third terms $(\boldsymbol{v}\cdot\nabla)\boldsymbol{v} + \nabla\Phi_g$ of the last expression of (6) correspond to the Christoffel-symbol terms of the geodesic curved motion of the covariant derivative as an extension of the partial derivative $\partial_t\boldsymbol{v}$. See Chap.12 of Misner *et al.* [15], and Appendix C of Kambe [4].

[9] $\mathcal{P} \equiv \rho h = (\rho\epsilon + p)$ is the *enthalpy* per unit volume, where ϵ and $h = \epsilon + p/\rho$ are termed the *internal energy* and *enthalpy* per unit mass. In the dissipation-free motion keeping the mass element $\mathcal{M} = \rho\,\mathrm{d}^3x$ fixed, the entropy s per unit mass is unchanged, and the variation of ϵ is given by $\mathrm{d}\epsilon = T\mathrm{d}s - p\,\mathrm{d}\rho^{-1} = -p\,\mathrm{d}\rho^{-1}$. Then, $\mathrm{d}h = \mathrm{d}(\epsilon + p/\rho) = \rho^{-1}\,\mathrm{d}p$. Then, $\mathrm{d}(\mathcal{P}\,\mathrm{d}^3x) = \mathcal{M}\mathrm{d}h$ reduces to $\mathrm{d}\mathcal{P} = \rho\,\mathrm{d}h$ per unit volume.

[10] Y. Sofue, PASJ **70**, 31 (2018).

[11] T. Kambe, GJSFR **22**, 61 (2022).

[12] G. Ludwig, Galactic rotation curve and dark matter according to gravitomagnetism, EPJC **81**, 186 (2021).

[13] $(\nabla \times \boldsymbol{b})_\phi = \partial_Z b_R - \partial_R b_Z = -R^{-1}\partial_Z^2 \Psi - \partial_R(R^{-1}\partial_R \Psi)$.

[14] With $n = 2$, the numerical analysis caused a complexity, while the correction terms vanish with the case of $n = 4$ on the plane $Z = 0$ and the numerical work succeeded in yielding the solution straightforwardly.

[15] C. Misner, K. Thorne, and J. Wheeler, *GRAVITATION* (Princeton University Press, 2017).

Note Added in Proof:

(I) Disk-Halo Con-spiracy in Silence

About the dark matter problem of spiral galaxies, *what is of primary importance* is the observational FACTS first: (*a*) *Neutral hydrogen* existing in the dark halo; (*b*) *Flatness* of the rotation curves; (*c*) *Disk-halo* conspiracy; (*d*) *Hyper-orbital-speeds* in the halo. Secondly, a new theoretical finding is presented in the main text, concerning the dynamical balance between the *gravitational force* and (a new) *fluid-Lorentz-force*. This provides a profound insight into the *Disk-Halo Con-spiracy in silence*.

The first indications that spiral galaxies are surrounded by *unseen dark objects* date back to the early seventies (Hoekstra *et al.* [1]). Subsequently, Bosma [2] confirmed evidence of existence of an HI-region by observing the 21-cm HI-line (hence optically *dark*) in 1981. The dark object manifests itself from *outer-most* parts of the luminous body toward the halo of spiral galaxies. Its remarkable signature lies in the *flatness* of the rotation curves observed well outside the luminous region.

The dark matter problem in the spiral galaxies concerns the outer regions beyond the optical disk. The disk plus the bulge consists a part of spiral galaxies on one hand, and the dark halo another. Both parts bring an essential and about-equal contribution to the flat rotation curve in two distinct regions, which are the inner *luminous* region on one hand and the outer HI region emitting the 21 cm line (hence *dark*) on the other. This observation implies a physical coupling called the *disk-halo conspiracy* [3].

A decade later, McGaugh-Lelli-Schoenbart [4] opened a door with an innovative diagram, illuminating the disc-halo conspiracy visually. They represented the observed statistics by a fitting curve $A_c = \mathcal{F}(A_g)$ given by (3) in the main text, warped upward toward smaller A_g. It expresses a relation between two *accelerations* A_c and A_g, where A_c is the centripetal acceleration of a body, either a star or a gas cloud, and A_g the gravitational acceleration, both directed toward the galactic center. The difference $A_{\rm DM} \equiv A_c - A_g$ is interpreted as that due to dark objects.

The new curve-representation has opened a door, which has enabled the present approach based on the dynamical equation. The dark matter issue is thus formulated mathematically, and the disk-halo conspiracy is represented with physical terms without presence of dark matters, enabling a mathematical interpretation on the disk-halo conspiracy.

What is understood at present is as follows. In the dark halo consisting of cold gases (including HI-gas), the orbital motion is characterized with hyper-velocities of $200 \sim 300$ km$\cdot$ s^{-1}. By the power of the hyper-speeds and the action of a physical an-isotropic stress field (*i.e.* fluid Lorentz force), the celestial objects in the dark halo are driven by the inner rotational currents of the spiral arms which are also orbiting at ultra-high speeds.

The Disk-Halo *Con-Spiracy* might be interpreted as follows. Strength of the gravitational force becomes weaker as the distance R from the center increases, while strength of the fluid-Lorentz-force grows towards the halo as R increases. Continuous shift in their relative influences and resulting role-switching are nothing but the Disc-Halo *Con-Spiracy*.

The present studies ([5], [6]) aim to investigate the aboves as targets. In compact terms, the study intends *Unlocking Galactic Mysteries*. A particularly notable finding is the excellent matching of the theoretical prediction with the observation, which implies that the present approach has captured an essential aspect of the Dark Matter effect. This match not only reveals surprising dynamical features of galaxies, but also asserts the validity of the new physical law described above as the *Fluid-Lorentz-Force*.

According to "*fluid-Lorentz-force*", the *orbital current* (electrically neutral) along the circular orbit $R = R_1$ acts as a source generating a *fluid gauge field*. The field thus generated (inside and outside R_1) acts on surrounding currents. Particularly, the *fluid-Lorentz-force* acting on the *outer* current at $R_2\,(> R_1)$ yields a force, not only *tightening* the *inner* currents, but also maintaining the *outer current* at R_2 without flying away.

The hyper orbital speed observed in the galactic halos is telling a true evidence that the Fluid-Lorentz-Force is working in real cosmic space.

(II) **Invisible gauge field $\boldsymbol{a}$ creating a visible effect in a twisting sense**

In order to get an insight into the role of the gauge field $\boldsymbol{a}$ introduced in the main text, the example of the Kundt-tube experiment [7] would be useful. In the Kundt's experiment, "*the gauge field within the acoustic-tube is not visible, yet creates visible dust-striations mechanically*". Correspondingly, the gauge field $\boldsymbol{a}$ generating the *Fluid Lorentz Force* in the galactic space has the same mechanical origin as that of Kundt's field. The difference lies in the spatial scale and also in whether there exists the gravity field or not. The study [5] investigated how to incorporate the gauge field of Fluid Dynamics of flat space into curved space with gravity.

The gravity field has an analogous aspect. *The gravitational potential Φ_g is not visible, yet its derivatives $\partial\Phi_g/\partial x^k$ create visible dynamical effect.* However, the gravity has an intrinsic dynamical property. In the relativistic formulation, the galactic space is curved by the presence of the gravitational potential Φ_g. The trajectory of motion of any celestial object with a mass is curved owing to the invisible gravitational potential.

The *fluid Lorentz force* depends on the cross-product $\boldsymbol{v}\times\boldsymbol{b}$, acting perpendicularly to the 3-velocity vector $\boldsymbol{v}$. This is contrasted with the gravity force $\boldsymbol{f}_g$, given by $\boldsymbol{f}_g = -\nabla\Phi_g$. In this regard, the action of $\boldsymbol{f}_L = \boldsymbol{v}\times\boldsymbol{b}$ is *twisted*. Namely, $\boldsymbol{f}_L$ acts on the body perpendicular to its velocity $\boldsymbol{v}$, unlike the gravity $\boldsymbol{f}_g$ acting anti-parallel to the scalar gradient.

[i] H. Hoekstra, T. S. van Albada and R. Sancisi, *MNRAS*, **323**, 453, (2001).
[ii] A. Bosma, *AJ*, **86**, 1825, (1981).
[iii] D. Pfenniger, F. Combes and L. Martinet, *A & A*, **285**, 79, (1994).
[iv] S. S. McGaugh, F. Lelli and M. Schombert,*PRL*, **117**, 201101, (2016).
[v] T. Kambe, *GJSFR*-A, **23** (8), 13-27, (2023).
[vi] T. Kambe and M.Hashiguchi *GJSFR*-A, **23** (10), 1 - 13, (2023).
[vii] T.Kambe, *GJSFR*-A, **22** (6), 61 - 86, (2022).